JOURNAL OF GEOPHYSICAL RESEARCH, VOL. 108, NO. D18, 4564, doi:10.1029/2002JD003217, 2003

Seasonal variations of the atmospheric temperature structure at South Pole

Weilin Pan[1] and Chester S. Gardner

Department of Electrical and Computer Engineering, University of Illinois at Urbana-Champaign, Urbana, Illinois, USA

Received 25 November 2002; revised 14 April 2003; accepted 10 June 2003; published 16 September 2003.

[1] Fe/Rayleigh lidar measurements are combined with the high-altitude balloonsonde data and used to characterize the seasonal variations of atmospheric temperature at South Pole from the surface (2.835 km) to 110 km altitude. Twelve-month oscillations, associated with solar UV absorption by ozone, dominate the seasonal variations of temperature throughout the stratosphere and lower mesosphere from 10 to 60 km. In the mesopause region between 70 and 100 km, 12- and 6-month oscillations dominate the seasonal variations with the warmest temperatures occurring near the spring and fall equinoxes. During the month of March, temperature near 80 km is more than 25 K warmer than MSIS-00. The spring and fall temperature maxima in the mesopause region appear to be associated with the combined effects of the annual variations in adiabatic heating and cooling and the annual variations in solar heating, which are 180° out of phase. During the month of June, the stratopause and mesopause temperatures are about 20–30 K colder than the model predictions. The seasonal temperature variations are the largest near 85 km altitude, where they are approximately 85 K peak to peak. *INDEX TERMS:* 0350 Atmospheric Composition and Structure: Pressure, density, and temperature; 1610 Global Change: Atmosphere (0315, 0325); 3319 Meteorology and Atmospheric Dynamics: General circulation; 3334 Meteorology and Atmospheric Dynamics: Middle atmosphere dynamics (0341, 0342); 3349 Meteorology and Atmospheric Dynamics: Polar meteorology; *KEYWORDS:* lidar, South Pole, middle atmosphere temperature

Citation: Pan, W., and C. S. Gardner, Seasonal variations of the atmospheric temperature structure at South Pole, *J. Geophys. Res.*, *108*(D18), 4564, doi:10.1029/2002JD003217, 2003.

1. Introduction

[2] Access to high-quality measurements of atmospheric parameters and constituents is essential for validating and calibrating modern global circulation models. Measurements of temperature, winds, and constituent profiles at the North and South Poles provide an especially convenient means of testing model calculations. Unfortunately, such observations are challenging and until recently, measurements of key parameters, such as temperature, have only been conducted in the troposphere and lower stratosphere at the poles with balloonsondes to altitudes below 30 km. While extensive temperature observations of the lower and middle atmosphere have been conducted at several high-latitude sites in the Arctic, little data are available from the Antarctic and until now, only a few airglow measurements have been made in winter at South Pole. The U.S. National Center for Environmental Prediction (NCEP) provides low resolution tropospheric and stratospheric temperatures derived from microwave sounding by polar orbiting satellites. However, none of these satellites can observe directly over the poles.

[3] Among the few reported middle atmosphere temperature observations in the Antarctic are the OH airglow measurements (~88 km) made by *Hernandez et al.* [1992] and *Greet et al.* [1994] at South Pole and Mawson (67.6°S), respectively. *Lübken et al.* [1999] reported rocket measurements of temperature profiles made in the upper mesosphere during late summer at Rothera (68°S). The only lidar measurements of temperature profiles above Antarctica have been limited to wintertime observations of the stratosphere at McMurdo Station (78°S, 167°E) made by *Di Donfrancesco et al.* [1996] and wintertime observations of the mesopause region at Syowa Station (69°S, 40°E) made by *Kawahara et al.* [2002].

[4] From December 1999 until October 2001, the University of Illinois lidar group operated an Fe/Rayleigh temperature lidar at the Amundsen-Scott South Pole Station [*Gardner et al.*, 2001]. This instrument was designed to make temperature profile measurements, during both day or night, from 30 km to as high as 110 km, depending on the mesospheric Fe concentrations [*Chu et al.*, 2002]. More than 1700 h of temperature, Fe density, and polar mesospheric cloud (PMC) observations were made with this lidar during its two year deployment at South Pole. *Pan et al.* [2002] reported the initial wintertime observations and showed that the stratopause and mesopause regions at South Pole are much colder during midwinter than current models predict. In this paper we characterize the seasonal variations of temperature structure above South Pole from the surface

[1]Now at SRI International, Menlo Park, California, USA.

0148-0227/03/2002JD003217$09.00

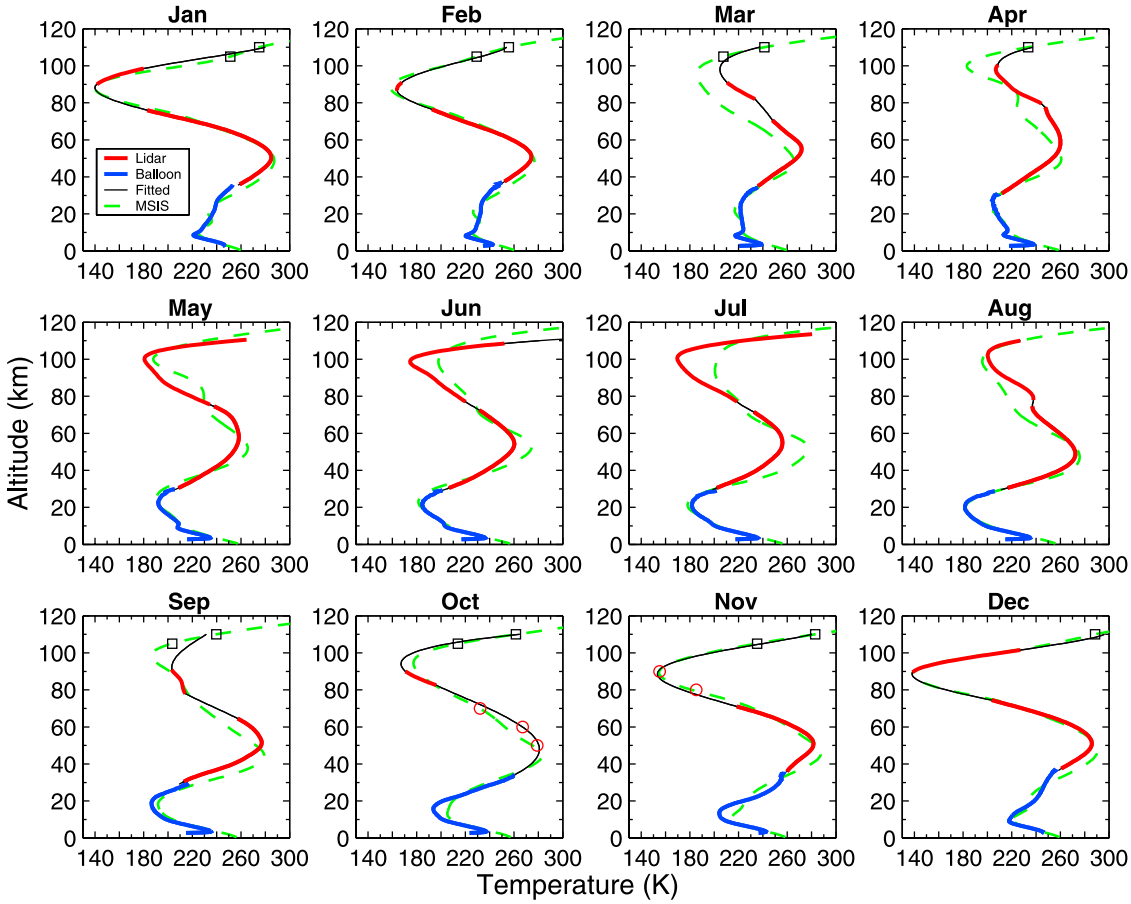

Figure 1. Observed and fitted monthly mean temperature profiles from the surface to 110 km at South Pole. Balloon data are plotted as solid blue curves, lidar data as solid red curves, MSIS-00 as dashed green curves, and the sixth-order polynomial fits as solid black curves. Supplemental data points used to constrain the polynomial fits are plotted as black squares (MSIS-00 data) and red circles (lidar data). The vertical resolution is 250 m for balloon data and 500 m for the rest.

to 110 km altitude throughout the year by combining the lidar data with ballonsonde measurements of the troposphere and lower stratosphere. We discuss the major features of this extensive data set and compare the observed temperatures with those predicted by MSIS-00 (Mass-Spectrometer-Incoherent-Scatter Model) [*Hedin*, 1991].

2. Observations

[5] Radiosonde balloons are launched daily at the Amundsen-Scott South Pole Station and tracked with a radio theodolite. Almost every flight is limited by catastrophic balloon failure and the maximum altitude varies from flight to flight. In winter balloon elasticity is severely reduced by the extremely cold lower stratosphere so that maximum altitudes are usually 15 km or less. To extend the maximum altitude to 25 km or higher, special 7000 in^3 balloons were substituted for the standard 600 in^3 balloons and launched twice weekly during the four year period 1993–1996 [*Pfenninger et al.*, 1999]. The payloads were the Atmospheric Instrumentation Research model IS-4A-1860 radiosondes. Pressure (0.01 mbar resolution, 0.1 mbar accuracy), temperature (0.01 K resolution, 0.5 K accuracy), and relative humidity (0.01% resolution, 3% accuracy) were sampled every 2–3 s during ascent and the altitude was derived from the pressure.

[6] Although balloonsonde data were available during the period of lidar deployment, the altitude coverage above 20 km was inadequate. Comparison of the 1993–1996 temperature profiles with those obtained during 1999–2001 showed that temperatures near 20 km were warmer by 5–20 K in October and November of 1999–2001 because stratospheric ozone levels were higher in the late 1990s. During the remainder of the year the two sets of data showed little differences in the weekly mean tropospheric and lower stratospheric temperatures.

[7] The monthly mean temperature profiles were computed using the 1993–1996 high-altitude balloon data. They are plotted as blue curves in Figure 1 at 250 m resolution along with the MSIS-00 model. The base altitude of the South Pole Station is 2.835 km. There is a persistent inversion layer near 3.5 km from February through November. Although the tropopause typically lies near 8 km, in winter the temperature continues to decrease with increasing altitude above the tropopause reaching a minimum near 20 km in the lower stratosphere.

[8] In November 1999 the University of Illinois Fe/Rayleigh lidar was installed in the Atmospheric Research

Table 1. Lidar Observation Periods for Data Used to Derive the Monthly Mean Temperature Profiles Plotted in Figure 1

	Jan.	Feb.	March	April	May	June	July	Aug.	Sept.	Oct.	Nov.	Dec.
Fe lidar												
Hours	13	4	18	6.3	7.5	3.5	5.5	9	11	2	n/a	9
Days	4	1	2	5	4	2	2	4	2	1	n/a	3
Rayleigh lidar												
Hours	257	120	66	51	31	25	23	22	9	n/a	117	226
Days	21	10	6	5	5	7	5	6	2	n/a	4	19

Laboratory, which is located 488 m north of the geographic South Pole [*Gardner et al.*, 2001]. The lidar can measure temperatures in the stratosphere and lower mesosphere using the Rayleigh technique and in the mesopause region and lower thermosphere using the Fe Boltzmann technique [*Gelbwachs*, 1994]. *Chu et al.* [2002] provided a detailed description of the instrument design and its temperature measurement capabilities. Although the Fe temperatures are usually derived between 80 and 105 km, observations as low as 76 km and as high as 114 km are sometimes possible in the austral winter [*Pan et al.*, 2002], while summertime measurements are limited by the low Fe densities and the high-level background noise from solar scattering. The accuracies for the observed Fe temperatures vary with altitude, resolution, and observing time. For a vertical resolution of 500 m and an observing period of 1 h, the accuracies are typically $\pm 3-5$ K at the peak of Fe layer depending on signal level, and ± 10 K at the upper and lower layer boundaries [*Chu et al.*, 2002].

[9] The molecular scattered lidar signal is proportional to atmospheric density. Temperatures can be derived from the relative density profile by integrating the profile downward using the hydrostatic equation, the ideal gas law, and a starting temperature at the highest altitude. Polar stratospheric clouds typically begin forming at South Pole between about 12 and 25 km in late May and persist until early September [*Collins et al.*, 1993]. To avoid errors associated with Mie scattering from these clouds, temperature profiles were derived from the molecular backscatter data only in the region between 30 and around 75 km.

[10] The monthly average Rayleigh and Fe temperature profiles are also plotted in Figure 1. The total observation time for each month is listed in Table 1. Only a subset of the lidar observations was used to derive the Fe temperatures in the mesopause region, so that the Fe hours are generally less than the Rayleigh hours. For example in January, a total of 13 hours of Fe lidar observations made on 4 different days were used to derive Fe temperature, while 257 hours of Rayleigh lidar observations made in 21 different days were used to derive Rayleigh temperature. Initially the Rayleigh temperature retrieval was seeded using the MSIS-00 temperature at $\sim$75 km (altitude varies depending on the lower boundary of Fe layer). Next a sixth-order polynomial was fitted to the balloon and lidar data between 25 km and 110 km to model the temperature profile. The Rayleigh temperature profile was then recomputed using the seed temperature predicted by the sixth-order polynomial and a new polynomial fit was computed. This process was repeated until the seed temperature predicted by successive fits differed by less than 0.5 K. The final polynomial, which characterizes the background temperature structure for the month, was then subtracted from the observed temperatures and the residuals were smoothed using a Hamming window with a full width at half maximum (FWHM) of 7.5 km. The smoothed residuals were added to the final polynomial and the results are plotted at 500 m resolution in Figure 1 as the red curves. At those altitudes where lidar observations are absent, the polynomial fit is plotted as the black curve.

[11] A sixth-order polynomial was used to characterize the background temperature structure because it provided excellent fits to the monthly mean temperature profiles predicted by MSIS-00 for the South Pole. The RMS difference between the monthly mean MSIS-00 temperatures profiles from 25 to 110 km and their polynomial fits falls rapidly with increasing fit order up to 6, while the improvement is marginal for orders higher than 6.

[12] The accuracies of the smoothed lidar temperature profiles vary with altitude and observation time for the month. The monthly mean profiles were derived by using Fe and Rayleigh temperature data for which the measurement errors were no larger than 15 K. The largest errors occur at the top and bottom edges of the Fe profiles and at the top of the Rayleigh profiles where the lidar signals are weakest. After smoothing with the 7.5 km FWHM Hamming window, the measurement error in the monthly mean lidar temperature profiles is reduced to less than about 3.5 K.

[13] During summer it was not possible to measure temperatures throughout the mesopause region and lower thermosphere with the Fe lidar even though the observation time was extensive. In summer the Fe densities at South Pole are low because of the extremely cold mesopause region temperatures. The layer is thin with the peak density near 92 km, while the region below 90 km is contaminated by the presence of PMCs. To constrain the polynomial fits, the spring, summer, and fall lidar observations were supplemented with MSIS-00 model temperatures at the highest altitudes in the lower thermosphere (viz., at 105 and 110 km). These temperature estimates are identified by the black squares in Figure 1. Similarly, in October and November, lidar coverage of the mesosphere is limited so the polynomial fits were constrained by employing the average of the temperatures observed at several selected altitudes between 50 and 90 km in the months before and after. These are identified as the red circles in Figure 1. Thus, by using the balloon observations near 25 km, MSIS-00 model predictions at 105 and 110 km in spring, summer, and fall, and lidar data in between, it was possible to obtain excellent polynomial fits to the mean monthly temperature profiles throughout the year between 25 and 110 km.

[14] The monthly mean lidar temperature profiles are combined with the weekly mean balloon profiles at 500 m resolution and are plotted in color contour format in Figure 2. The temperatures predicted by the sixth-order polynomial fits are plotted at those altitudes not covered by balloon data or by the Rayleigh and Fe lidar measurements (see Figure 1). At those altitudes covered by balloon and

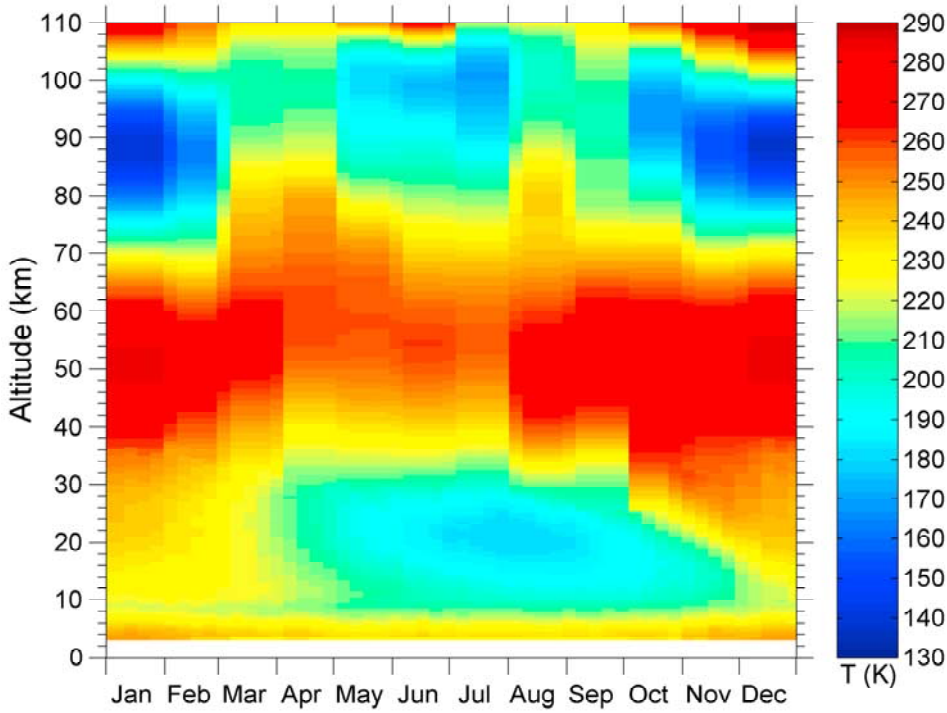

Figure 2. Combined weekly mean balloon temperatures and monthly mean lidar temperatures, with the sixth-order polynomial fits filling in the gaps. For weeks spanning two consecutive months, the temperatures are interpolated using the monthly mean temperatures at those altitudes not covered by weekly balloon data. The vertical resolution is 500 m.

lidar measurements, the accuracies of the mean temperatures are ±3.5 K or better.

3. Seasonal Temperature Variations

[15] To characterize the seasonal variations in the temperature structure between 3 and 110 km, 12-, 6-, 4-, 3-, and 2.4-month sinusoidal oscillations were fitted to the data in Figure 2. These frequency components were identified to be dominant by analyzing the power spectral density (PSD) of the weekly temperature data. The fits were computed sequentially. First, the 12-month fit was computed and then subtracted from the raw data before the 6-month fit was computed. The 6-month fit was then subtracted before the 4-month fit was computed and so on. The resulting amplitude and phase profiles are plotted as solid curves in Figure 3. Also plotted for comparison as dashed curves, are the parameters from the corresponding fits to the MSIS-00 model. The accuracies of the harmonic amplitudes are ±1.5 K or better. The phase accuracies depend on the harmonic amplitudes. When the harmonic amplitude is 2 K or larger, the phase accuracy is ±11% of the period or better. The amplitudes of the 4-, 3-, and 2.4-month variations are comparable to the 6-month amplitudes below 70 km while the MSIS-00 model exhibits negligible variations at these timescales. Because the harmonic analysis employed monthly mean temperature data above 25 km, the amplitudes of the 4-, 3-, and 2.4-month variations may be even larger than the values plotted in Figure 3.

[16] In the stratosphere the maximum amplitude of the 12-month variations exceeds 30 K with the warmest temperatures occurring in December and January. In the mesopause region, the 12-month amplitude is also near 30 K at 85 km but the warmest temperatures occur in June. The data are generally consistent with the MSIS-00 variations except near 85 km where the amplitudes of the MSIS-00 12-month variations approach 40 K, about 10 K larger than the observational data. The 6-month amplitudes of the observational data are less than 5 K below 65 km but reach almost 25 K between 80 and 90 km. The 6-month temperature oscillations are warmest in March and September at the beginning and end of the austral winter. The amplitudes of the MSIS-00 6-month oscillations are about double those of the observational data in the stratopause region and more than 5 K smaller in the mesopause region.

4. University of Illinois South Pole Temperature Model

[17] To further characterize the temperature structure at South Pole, the mean plus 12- and 6-month harmonic variations were computed at each altitude between 3 and 110 km using the weekly mean balloon and monthly mean lidar profiles in Figure 2. The mean plus harmonic fits were subtracted from the observed temperature time series and the residual variations were smoothed using a Hamming window with a time resolution of 1 week and a FWHM of 6 weeks. This further reduces measurement errors and largely eliminates temporal variations with periods of two months or less. Smoothing also attenuates the amplitudes of the 4-, 3-, and 2.4-month oscillations plotted in Figure 3. The smoothed residuals were then added to the mean plus 12- and 6-month fits. The resulting weekly mean temperature profiles are plotted in color contour format in Figure 4.

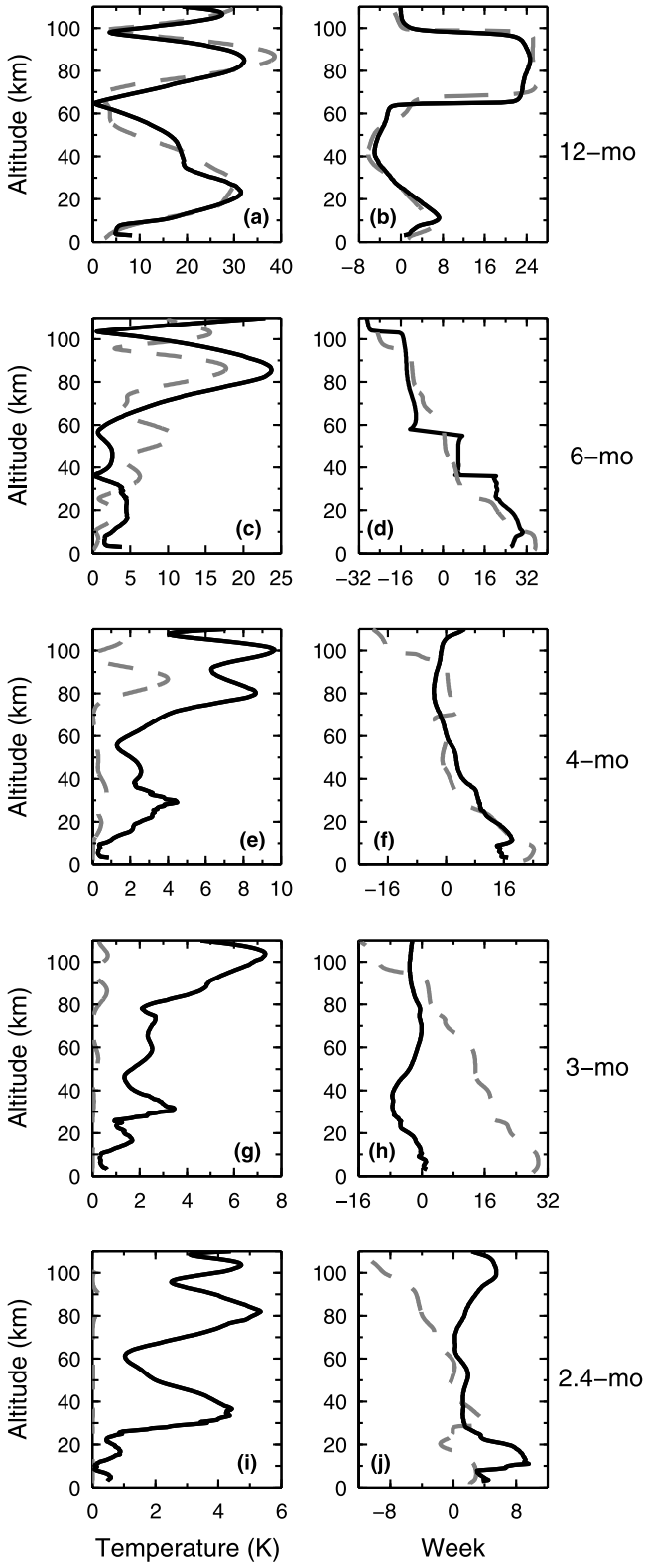

Figure 3. Altitude profiles of the (a) 12-month amplitude, (b) 12-month phase, (c) 6-month amplitude, (d) 6-month phase, (e) 4-month amplitude, (f) 4-month phase, (g) 3-month amplitude, (h) 3-month phase, (i) 2.4-month amplitude, and (j) 2.4-month phase (all in solid curves) computed from the balloon/lidar temperature data in Figure 2 and from the MSIS-00 model (dashed curves).

These data comprise the University of Illinois South Pole temperature model which we denote UISP-02. At those altitudes covered by balloon and lidar measurements, the accuracies of the temporally smoothed temperatures are ±3 K or better.

5. Comparison With MSIS-00

[18] The MSIS empirical model was originally developed to simulate the temperature, density, and composition in the thermosphere. After releasing several improved versions of the model, *Hedin* [1991] extended the model downward to the mesosphere and below, by incorporating zonal mean satellite data between 80°S and 80°N below 72.5 km from MAP (Middle Atmosphere Program) Handbook [*Barnett and Corney*, 1985], and by supplementing the harmonics analysis of NMC (National Meteorological Center) data below 20 km. In addition, other historical data were taken into account, such as rocketsondes and balloonsondes. The most recent update, MSIS-00 model, is capable of providing detailed predictions of temperature, pressure, and density in the atmosphere from 0 to 250 km as a function of location, season, and time of day. However, the current MSIS model has the poorest data coverage at high-latitude mesosphere and above, especially in the Southern Hemisphere where observational data south of 80°S is virtually non-existent.

[19] To compare our observational data with the MSIS model, we subtracted the weekly mean MSIS-00 temperature profiles from the corresponding UISP-02 profiles. The difference is plotted in color contour format against altitude and month in Figure 5b. The RMS difference is also plotted against altitude in Figure 5a. Starting as early as 1957, meteorological balloon soundings have been routinely made at South Pole providing extensive data for empirical models such as MSIS-00. Not surprisingly, the balloon data below 30 km used in the UISP-02 model shows the least deviation from the MSIS-00 model except for the ∼10 K temperature discrepancies during October and November. This appears to be caused by the different ozone concentration from year to year, while current MSIS-00 model does not include any year information. In this region, the RMS difference averages about 5 K except near the surface where MSIS-00 does not accurately model the extremely cold boundary layer temperatures at South Pole. At altitudes between 40 and 60 km, the RMS temperature differences of ∼10 K are mainly caused by the colder stratospheric winter resulting from weaker than expected compressional heating associated with the meridional circulation system [*Pan et al.*, 2002]. The RMS difference is about 15 K near the mesopause region, where UISP-02 is considerably warmer than MSIS-00 in March and considerably colder in midwinter [*Pan et al.*, 2002].

6. Discussion

[20] Because the South Pole is located near the center of the high featureless Antarctic Plateau, frontal activity is virtually nonexistent. Diurnal and tidal variations are also minimal since the atmosphere is constantly illuminated by the Sun in summer and in complete darkness during the 6-month winter. The balance between solar heating, chemical heating, radiative cooling, and adiabatic cooling

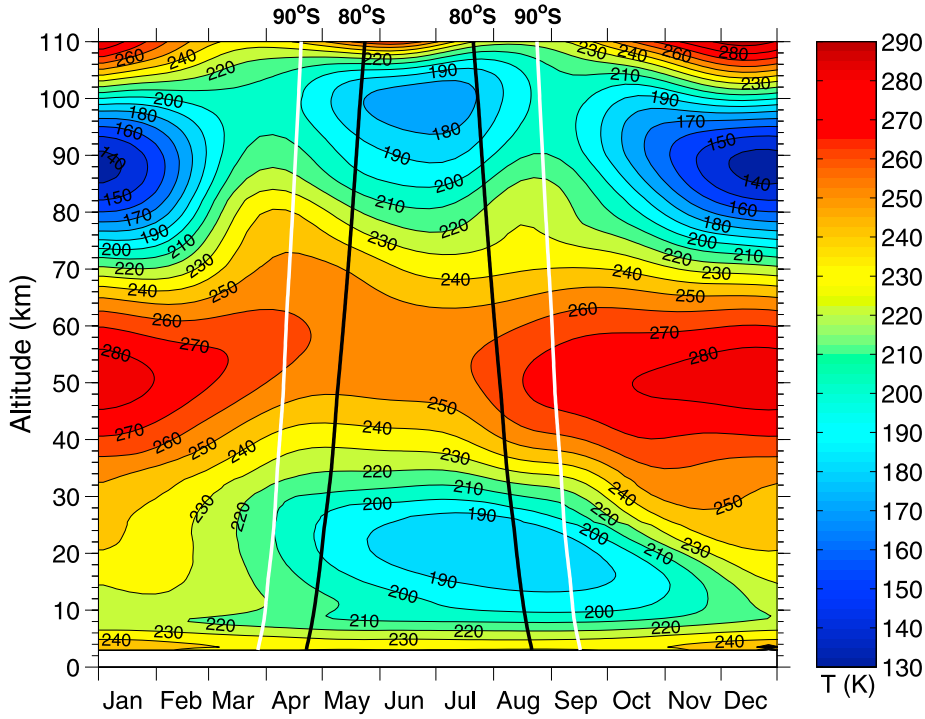

Figure 4. The observed weekly mean temperature structure of the atmosphere above South Pole (UISP-02) plotted from 3 to 110 km. Polar nights (24 h darkness) occur between the white curves at 90°S and between the black curves at 80°S. The vertical resolution is 500 m.

associated with upwelling over the polar cap in summer, largely determines the summertime temperature structure from the upper stratosphere to the lower thermosphere above the South Pole. In winter when solar heating is absent, the balance between chemical heating, radiative cooling, and adiabatic heating associated with subsidence over the polar cap determines the temperature structure. These effects alone account for the dominant seasonal variations exhibited by the UISP-02 model plotted in Figure 4.

[21] By taking the time derivative of the UISP-02 temperatures, the net heating/cooling rates were calculated at each altitude and the results are plotted in color contour format in Figure 6b. The RMS variations of the heating/cooling rates are also plotted in Figure 6a. The greatest variability occurs

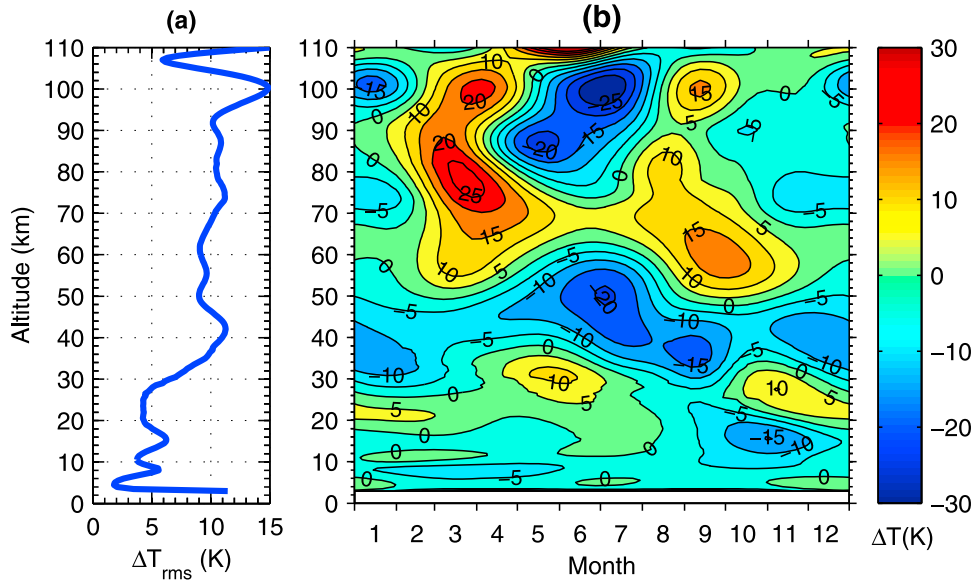

Figure 5. (a) RMS and (b) absolute temperature differences (UISP-02 minus MSIS-00) between the MSIS-00 model and the UISP-02 observational model. The vertical resolution is 500 m.

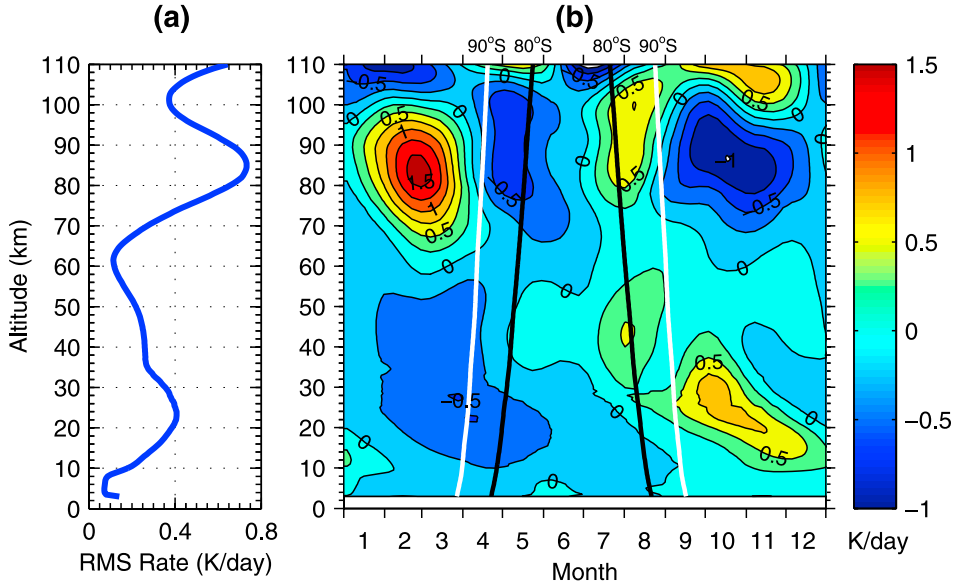

Figure 6. (a) RMS and (b) weekly heating/cooling rates derived from the UISP-02 observational data. Polar nights (24 h darkness) occur between the white curves at 90°S and between the black curves at 80°S. The vertical resolution is 500 m.

at 23.5 and 85 km. Listed in Table 2 are the observed net total heating/cooling rates at 50 and 85 km for solstices and equinoxes, along with the estimated solar heating, chemical heating, infrared cooling, and adiabatic heating/cooling rates.

[22] The estimated solar heating rates were adopted from Figure 1 of *Fomichev and Shved* [1988] representing the thermal energy portion of the absorbed solar radiation by (1) O_2 in the Schumann-Runge continuum and bands and the Herzberg continuum, (2) O_3 in the Hartley bands, the Huggins bands, and the Chappuis bands, (3) CO_2 and H_2O in the infrared vibration-rotation bands. As expected, the solar heating peaks in midsummer, decreases quickly after sunset and is negligible in midwinter.

[23] The chemical heating rates in Table 2 were estimated by only considering the exothermic reaction between atomic hydrogen and ozone, which has been identified as potentially the largest single chemical heat source in the mesopause region by *Mlynczak and Solomon* [1991, 1993]. The heating rate was computed using the reaction rate and heating efficiency from *Mlynczak and Solomon* [1991, 1993], our UISP-02 temperature, the concentration of H taken from the MSIS-00 model, and the ozone mixing ratio taken from *Fomichev et al.* [1986].

[24] The infrared cooling rates in Table 2 include contributions from (1) the 15-μm CO_2 band (calculated based on UISP-02 temperatures using the matrix parameterization proposed by *Fomichev et al.* [1998] at 360 ppm mixing ratio [*Gillette et al.*, 1987], and (2) the 9.6-μm O_3 and the rotational H_2O bands (interpolated from Figures 11–14 of *Fomichev et al.* [1986]). Infrared cooling is temperature dependent and therefore varies with the season.

[25] The adiabatic heating/cooling rates were computed as the product of vertical wind and the difference between dry adiabatic and UISP-02 lapse rates [*Holton*, 1992]. The vertical wind data were taken from the Thermosphere-Ionosphere-Mesosphere-Electrodynamics Global Circulation Model (TIME-GCM) [*Roble and Ridley*, 1994]. By subtracting radiative, chemical, and adiabatic rates from the observed net total rates, the unaccounted heating/cooling rates are summarized in Table 2. This analysis suggests that more detailed modeling of the various heat sources and sinks is required to bring the computed rates in better agreement with observations.

[26] In late March and early April when the Sun sets on the atmosphere above the South Pole (white curve labeled 90°S in Figure 4), the stratosphere and mesosphere rapidly cool largely through the emission of thermal radiation and this helps establish the circumpolar belt of westerly winds known as the polar vortex [*Schoeberl and Hartmann*, 1991]. The vortex inhibits the transport of warmer air from lower

Table 2. Atmospheric Thermal Budget at 50 and 85 km[a]

Heating/Cooling Rate, K/day	December		March		June		September	
	50 km	85 km	50 km	85 km	50 km	85 km	50 km	85 km
Solar heating	16.0	8.0	2.4	1.5	0	0	2.6	1.5
Chemical heating	0	2.8	0	1.5	0	0.8	0	1.3
Infrared cooling	−11.0	4.4	−8.9	−7.3	−7.6	−2.4	−11.3	−4.9
Adiabatic	−1.1	−21.9	5.5	−0.2	9.3	2.1	7.4	0.6
Unaccounted	−3.9	6.5	0.6	5.4	−1.7	−0.6	1.4	0.8
Observed net total	0	−0.2	−0.4	0.9	0	−0.1	0.1	−0.7

[a]Positive numbers represent heating, and negative numbers represent cooling.

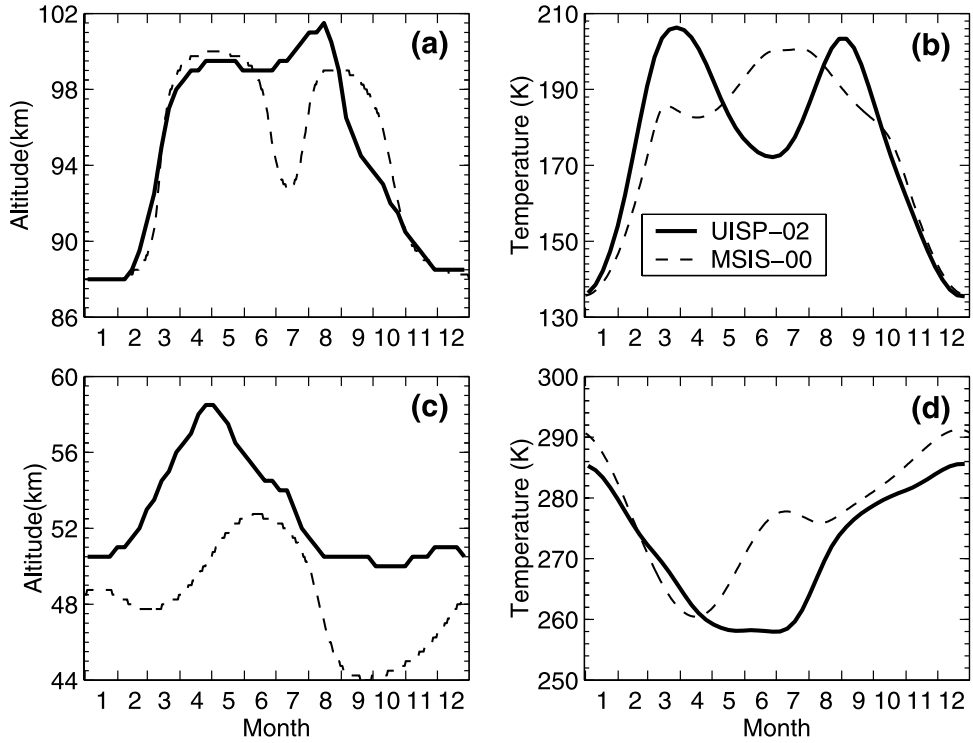

Figure 7. Seasonal variations of the (a) mesopause altitude, (b) mesopause temperature, (c) stratopause altitude, and (d) stratopause temperature at South Pole. The weekly UISP-02 data are plotted as solid curves, and the daily MSIS-00 model data are plotted as dashed curves.

latitudes into the polar cap. The wintertime radiative cooling is accompanied by strong downwelling over the south polar cap and weak upwelling elsewhere. The downwelling heats the atmosphere through adiabatic compression and partially offsets the effects of radiative cooling. This results in relatively warm south polar temperatures in winter and explains the existence of a stratopause in a region where solar heating is absent.

[27] UISP-02 shows that both the stratopause and mesopause regions are much colder during midwinter than MSIS-00. Comparisons of our monthly mean temperature profiles with the TIME-GCM model also show that the observed midwinter temperatures between 30 and 100 km are much colder than model predictions [*Pan et al.*, 2002]. These results suggest that compressional heating associated with subsidence over the polar cap is much weaker than expected. It is difficult to accurately model this process because it involves the modulation of the meridional circulation system by the sporadic generation of planetary and gravity waves in the lower atmosphere and their dissipation in the middle atmosphere [*Garcia and Boville*, 1994]. Modeling experiments conducted with TIME-GCM suggest that wintertime gravity wave forcing may be smaller than expected in the Southern Hemisphere. This results in weaker subsidence, weaker compressional heating, and colder stratopause and mesopause temperatures similar to those observed at South Pole [*Pan et al.*, 2002].

[28] The weekly mesopause and stratopause altitudes and temperatures are plotted in Figure 7. The stratopause increases in altitude starting in early February and reaches a maximum height of about 58 km in late April. The height appears to change in response to the setting Sun. In late March the troposphere and lower stratosphere is in complete darkness while the region above 55 km is illuminated until mid-April. This shadowing of the atmosphere by the Earth as the Sun sets distorts the temperature profile. As the lower stratosphere begins cooling after the Sun sets in late March, the stratopause moves rapidly upward until it also is in darkness by late April. The height then decreases throughout the winter. By early August the stratopause height is near 50 km when it is comparable to that predicted by MSIS-00. The mesopause exhibits a similar behavior but its height variations are largely controlled by the summer-to-winter transition associated with the meridional circulation system. Adiabatic cooling associated with upwelling during summer over the polar cap cools the region near 90 km to extremely low temperatures. As the upwelling weakens in late summer, the region near 90 km warms and the mesopause height increases rapidly from about 88 km to the winter state near 100 km.

[29] After sunset, both the stratopause and mesopause temperatures decrease, reaching minimum values in June near winter solstice. In midwinter, temperatures throughout the stratosphere and mesosphere are determined by the balance between radiative cooling, chemical heating, and compressional heating associated with subsidence over the polar cap. The minimum stratopause and mesopause temperatures are approximately 20 K colder than MSIS-00. As mentioned above, this appears to be a consequence of the weaker than expected subsidence resulting from weaker gravity wave forcing in the Southern Hemisphere during winter [*Pan et al.*, 2002; *Kawahara et al.*, 2002]. At 80°S,

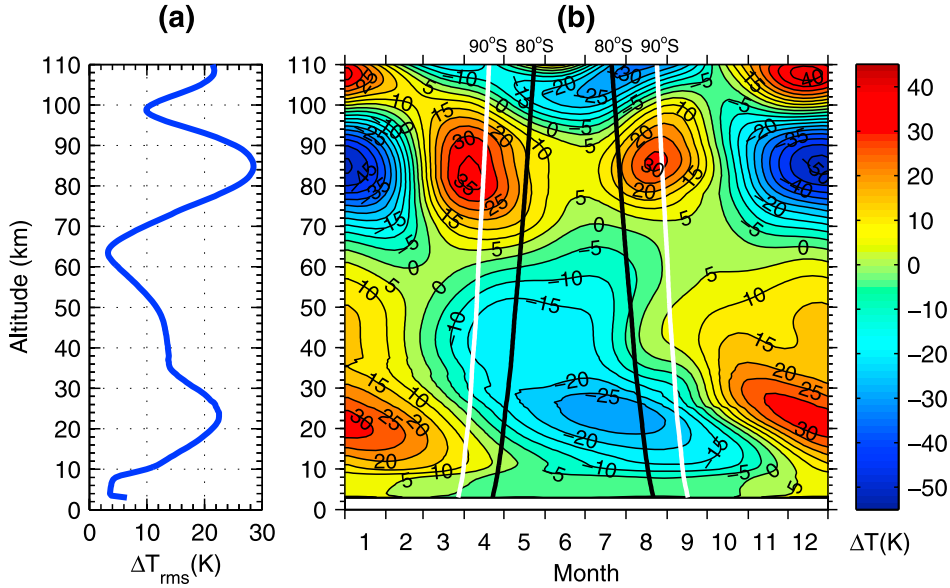

Figure 8. Seasonal variations of the South Pole temperature structure computed by subtracting the observed annual mean temperature from UISP-02: (a) RMS and (b) absolute variations. Polar nights (24 h darkness) occur between the white curves at 90°S and between the black curves at 80°S.

the Sun first rises around 24 July at 100 km altitude and around 5 August at 50 km altitude. In late winter, as the polar cap receives its first sunlight and subsidence begins to weaken, the stratopause and mesopause temperatures begin increasing. Below 95 km in the mesosphere and stratosphere, ozone absorption of UV radiation at wavelengths in the Hartley band between 200 and 300 nm is the main source of solar heating. Above 95 km the absorption of solar UV radiation by molecular oxygen in the Schumann-Runge bands and continuum (135–200 nm) and the Lyman-α line (121.5 nm) is the dominant heat source. In response to solar heating, the stratopause temperature increases throughout the spring and summer but remains colder than MSIS-00 until late January.

[30] As shown in Figure 5, the region between about 50 and 100 km is 5 to 20 K warmer during the springtime than MSIS-00. The atmosphere in this region, as well as the mesopause temperature, appears to respond more rapidly to the increasing solar radiation than MSIS-00 and TIME-GCM predict. On the basis of these observations, *Pan et al.* [2002] suggest that IR heating by CO_2 absorption in the 2.0-, 2.7-, and 4.3-μm wavelengths may also be important to the thermal balance of the mesosphere. The mesopause temperature reaches a local maximum near spring equinox and then falls rapidly as the upwelling associated with the meridional circulation cools the mesopause region to extremely low summertime temperatures.

[31] In summer, Rayleigh lidar coverage of the stratosphere is excellent while the low Fe densities and the presence of PMCs limit temperature coverage of the mesopause region. Above 60 km MSIS-00 and UISP-02 yield comparable temperatures through November, December, January, and February, although there were no mesopause region measurements in Nov and only limited altitude coverage in December, January, and February (see Figure 1). In March, as the adiabatic cooling associated with upwelling weakens and then ceases, the UISP-02 mesospheric temperatures are considerably warmer (25 K or more) than MSIS-00. We believe this may be associated with stronger than expected solar heating, perhaps by IR absorption by CO_2 [*Fomichev et al.*, 1998], and perhaps, weaker than expected upwelling strength.

[32] In the stratosphere, temperatures are dominated by the annual cycle of strong solar UV heating by ozone absorption in the summer and relatively weak compressional heating in the winter balanced by strong radiative cooling by CO_2 at all times of the year. Temperatures are coldest just after winter solstice and warmest near summer solstice. In the mesopause region temperatures are dominated by 12- and 6-month variations with the warmest temperatures occurring near the spring and fall equinoxes and the coldest occurring near the summer and winter solstices. In midsummer, adiabatic cooling dominates the mesopause region, yielding extremely low temperatures. In late summer, after upwelling over the polar cap ceases, the mesopause region is rapidly warmed by solar UV absorption by ozone and atomic oxygen. After the Sun sets following the fall equinox, radiative cooling by CO_2 dominates and is balanced by chemical heating and compressional heating in midwinter only after temperatures fall by more than 30 K below their fall maxima. In late winter and early spring after the Sun rises over the polar cap, the region is again warmed by solar heating and temperatures rise until upwelling begins to cool the upper mesosphere appreciably in late spring and summertime.

[33] The annual mean temperature profile was subtracted from UISP-02 and the differences are plotted against altitude and month in color contour format in Figure 8b to assess the annual variability. The RMS annual variation is plotted against altitude in Figure 8a. The variations are maximum at 85 km in the mesopause region, where they are ~85 K peak to peak, and at 23.5 km in the middle

stratosphere, where they are ~60 K peak to peak. Interestingly, these extreme temperature variations occur at the same altitudes of extreme heating/cooling rate variations (Figure 6a). Those are also the same altitudes where polar mesospheric clouds form in summer [*Chu et al.*, 2001a, 2001b] and polar stratospheric clouds form in winter [*Collins et al.*, 1993] above the South Pole.

[34] The annual variations reach local minima in the troposphere above the boundary layer, near 65 km in the lower mesosphere, and at 100 km near the boundary between the mesosphere and thermosphere. At these altitudes the RMS annual temperature variations are less than 10 K. At 65 and 100 km the annual variations in solar heating, chemical heating, and radiative cooling appear to almost perfectly balance the annual variations in adiabatic cooling and heating so that the temperatures here remain relatively constant throughout the year.

7. Conclusions

[35] By combining Fe/Rayleigh lidar and balloonsonde observations of the atmosphere made throughout the year, we have been able to characterize the seasonal variations of the temperature structure from the surface into the lower thermosphere at South Pole. Although high-altitude lidar coverage above 70 km was limited during summer when the Fe densities were low and the background noise from solar scattering was high, the data were sufficient to characterize the dominant 12- and 6-month oscillations in the temperature profiles. The data show that the stratosphere and lower mesosphere between 10 and 60 km altitude are dominated by a 12-month oscillation, with the coldest temperatures in winter when solar heating is absent. The data also show that wintertime temperatures in the mesopause and stratopause regions are 20–30 K colder than current model predictions. These differences appear to be caused by weaker than expected compressional heating associated with subsidence over the polar cap. The mesopause region between 70 and 100 km is dominated by 12- and 6-month temperature oscillations with maximum temperatures during the spring and fall equinoxes. The rapid response of this region to temperature changes as the Sun rises and sets suggests that solar heating is stronger and upwelling is weaker than current model predictions.

[36] **Acknowledgments.** The authors thank Xinzhao Chu, George Papen, and the two winter-over scientists, Ashraf Eldakrouri and John Bird, for their help installing and operating the Fe lidar at the Amundsen-Scott South Pole Station. The development, deployment, and operation of the University of Illinois Fe lidar at South Pole were supported by the National Science Foundation. To facilitate comparisons of our South Pole temperature data with model predictions and other measurements, the data plotted in Figures 1, 2, 4, and 6 can be downloaded at full resolution from our University of Illinois web site (http://conrad.csl.uiuc.edu/Research/SouthPole/).

References

Barnett, J., and M. Corney, Middle atmosphere reference model derived from satellite data, *Handb. MAP*, *90*, 47–85, 1985.

Chu, X., C. S. Gardner, and G. Papen, Lidar observations of polar mesospheric clouds at South Pole: Seasonal variations, *Geophys. Res. Lett.*, *28*, 1203–1206, 2001a.

Chu, X., C. S. Gardner, and G. Papen, Lidar observations of polar mesospheric clouds at South Pole: Diurnal variations, *Geophys. Res. Lett.*, *28*, 1937–1940, 2001b.

Chu, X., W. Pan, G. C. Papen, C. S. Gardner, and J. A. Gelbwachs, Fe Boltzmann temperature lidar: Design, error analysis, and initial results at the North and South Poles, *Appl. Opt.*, *41*, 4400–4410, 2002.

Collins, R. L., K. P. Bowman, and C. S. Gardner, Polar stratospheric clouds at the South Pole in 1990: Lidar observations and analysis, *J. Geophys. Res.*, *98*, 1001–1010, 1993.

Di Donfrancesco, G., A. Adriani, G. P. Gobbi, and F. Congeduti, Lidar observations of stratospheric temperature above McMurdo Station, Antarctica, *J. Atmos. Terr. Phys.*, *58*, 1391–1399, 1996.

Fomichev, V. I., and G. M. Shved, Net radiative heating in the middle atmosphere, *J. Atmos. Terr. Phys.*, *50*, 671–688, 1988.

Fomichev, V. I., G. M. Shved, and A. A. Kutepov, Radiative cooling of the 30–110 km atmospheric layer, *J. Atmos. Terr. Phys.*, *48*, 529–544, 1986.

Fomichev, V. I., J.-P. Blanchet, and D. S. Turner, Matrix parameterization of the 15 μm CO_2 band cooling in the middle and upper atmosphere for variable CO_2 concentration, *J. Geophys. Res.*, *103*, 11,505–11,528, 1998.

Garcia, R. R., and B. A. Boville, "Downward control" of the mean meridional circulation and temperature distribution of the polar winter stratosphere, *J. Atmos. Sci.*, *51*, 2238–2245, 1994.

Gardner, C. S., G. C. Papen, X. Chu, and W. Pan, First lidar observations of middle atmosphere temperatures, Fe densities, and polar mesospheric clouds over the North and South Poles, *Geophys. Res. Lett.*, *28*, 1199–1202, 2001.

Gelbwachs, J. A., Iron Boltzmann factor lidar: Proposed new remote-sensing technique for mesospheric temperature, *Appl. Opt.*, *33*, 7151–7156, 1994.

Gillette, D. A., W. D. Komhyr, L. S. Waterman, L. P. Steele, and R. H. Gammon, The NOAA/GMCC continuous CO_2 record at the South Pole, 1975–1982, *J. Geophys. Res.*, *92*, 4231–4240, 1987.

Greet, P. A., J. Innis, and P. L. Dyson, High-resolution Fabry-Perot observations of mesospheric OH (6-2) emissions, *Geophys. Res. Lett.*, *21*, 1153–1156, 1994.

Hedin, A. E., Extension of the MSIS thermospheric model into the middle and lower atmosphere, *J. Geophys. Res.*, *96*, 1159–1172, 1991.

Hernandez, G., R. W. Smith, and J. F. Conner, Neutral wind and temperature in the upper atmosphere above South Pole, Antarctica, *Geophys. Res. Lett.*, *19*, 53–56, 1992.

Holton, J. R., *An Introduction to Dynamic Meteorolgy*, 3rd ed., 511 pp., Academic, San Diego, Calif., 1992.

Kawahara, T. D., T. Kitahara, F. Kobayashi, Y. Saito, A. Nomura, C.-Y. She, and D. A. Krueger, Wintertime mesopause temperatures observed by lidar measurements over Syowa Station (69°S, 39°E), Antarctica, *Geophys. Res. Lett.*, *29*(15), 1709, doi:10.1029/2002GL015244, 2002.

Lübken, F.-J., M. J. Jarvis, and G. O. L. Jones, First in situ temperature measurements at the Antarcitic summer mesopause, *Geophys. Res. Lett.*, *26*, 3581–3584, 1999.

Mlynczak, M. G., and S. Solomon, Middle atmosphere heating by exothermic chemical reactions involving odd-hydrogen species, *Geophys. Res. Lett.*, *18*, 37–40, 1991.

Mlynczak, M. G., and S. Solomon, A detailed evaluation of the heating efficiency in the middle atmospheres, *J. Geophys. Res.*, *98*, 10,517–10,541, 1993.

Pan, W., C. S. Gardner, and R. G. Roble, The temperature structure of the winter atmosphere at South Pole, *Geophys. Res. Lett.*, *29*(16), 1802, doi:10.1029/2002GL015288, 2002.

Pfenninger, M., A. Z. Liu, G. C. Papen, and C. S. Gardner, Gravity wave characteristics in the lower atmosphere at south pole, *J. Geophys. Res.*, *104*, 5934–5984, 1999.

Roble, R. G., and E. C. Ridley, A thermosphere-ionosphere-mesosphere-electrodynamics general circulation model (time-GCM): Equinox solar cycle minimum simulations (30–500 km), *Geophys. Res. Lett.*, *21*, 417–420, 1994.

Schoeberl, M. R., and D. L. Hartmann, The dynamics of the stratospheric polar vortex and its relation to springtime ozone depletions, *Science*, *251*, 46–52, 1991.

C. S. Gardner, Department of Electrical and Computer Engineering, University of Illinois at Urbana-Champaign, 1308 West Main Street, Urbana, IL 61801, USA. (cgardner@uillinois.edu)

W. Pan, SRI International, 333 Ravenswood Avenue, Menlo Park, CA 94025, USA. (weilin.pan@sri.com)